

# Breakdown of the Macrospin Picture in Magnetodynamics from Spin Valves

F. Wegelin<sup>1</sup>, D. Valdaitsev<sup>1</sup>, A. Krasnyuk<sup>1</sup>, S. A. Nepijko<sup>1</sup>, G. Schönhense<sup>1</sup>, H. J. Elmers<sup>1</sup>, I. Krug<sup>2</sup>, and C. M. Schneider<sup>2</sup>

<sup>1</sup> Inst. f. Physik, Universität Mainz

<sup>2</sup> IFF-9: Electronic Properties

**Magnetic coupling effects play a fundamental role in the dynamic behavior of magnetic layer structures. Using time-resolved photoemission microscopy we measured the time-dependent spatial magnetization distribution in micron-sized spin valve structures in response to ultrashort magnetic field pulses. Quantitatively analyzing the magnetization dynamics we find that although the averaged magnetization vector reacts to the excitation according to a single-spin model with critical damping, local modes are excited depending on the shape of the spin valve structure.**

56 | 57

A spin valve (SV) represents a basic magnetic device structure being widely employed in sensors and hard disk read heads. Its functionality depends on the interplay of magnetic coupling phenomena. The simplest SV comprises two ferromagnetic (FM) layers separated by a non-magnetic (NM) spacer, which mediates an *indirect exchange coupling* [1]. More sophisticated structures fix the magnetization in one of the FM layers (hard layer) by a strong coupling (*exchange biasing*) to an antiferromagnet. In addition, further coupling mechanisms such as Néel and edge coupling may be at work. Thus, spin valves are extremely interesting structures from a fundamental point of view, providing unique access to the interplay of different types of magnetic coupling.

Often the dynamic behavior of the magnetization  $\vec{M}(t)$  is treated within the “macrospin” (MS) picture, assuming a uniform precessional motion of  $\vec{M}$ . Quantitatively, the magnetodynamic response may be described by the Landau-Lifshitz-Gilbert (LLG) equation,  $d\vec{M}/dt = -\gamma(\vec{M} \times \vec{H}_{\text{eff}}) + (\alpha/M_s)(\vec{M} \times d\vec{M}/dt)$ , with the gyromagnetic ratio  $\gamma$ , the Gilbert damping parameter  $\alpha$ , and the saturation magnetization  $M_s$ . The effective field  $\vec{H}_{\text{eff}}$  contains all coupling contributions and exerts a torque on  $\vec{M}$ , which initiates its precessional motion. For microscopic elements with small magnetic anisotropy and well-defined shape, however, the high-frequency behavior has been shown to be governed by confined spin wave eigenmodes [2].

In order to shed light on the dynamic response of coupled layer systems we explored the magnetodynamics in a dedicated spin valve [3]. The sample

studied comprises an advanced layer structure designed to optimize the GMR effect [4, 5] (courtesy of NAOMI/Sensitec, Mainz). The SV layer stack was grown on Cu films (100 nm) on Si(111) substrates. Subsequent lithography steps defined the final structure of a coplanar Cu waveguide (20  $\mu\text{m}$  central lead width) with microscopic SV elements of several shapes on top. In the SV a magnetically soft CoFe/NiFe free layer is separated from the CoFe hard layer by an ultrathin Cu interlayer providing an antiferromagnetic coupling field of 0.6 mT, as derived from the easy axis loop in conventional magnetometry ( $H||y$ ). Corresponding hard axis ( $H||x$ ) loops reveal a nearly reversible magnetization rotation, their initial slope indicating a total anisotropy field of 1.5 mT. The difference might be ascribed to a magnetic field-grown related uniaxial anisotropy.

For a quantitative analysis of the magnetization dynamics in these micro-elements we mapped the temporal evolution of the magnetization pattern using a pump-probe imaging approach based on photoemission electron microscopy [6]. The sample was illuminated with circularly polarized X-ray pulses ( $\Delta t = 3$  ps, repetition rate 500 MHz) from BESSY II. The magnetic contrast was derived from magnetic X-ray circular dichroism (MXCD) at the Ni  $L_3$  absorption edge. In this way, the response of the element was probed via the SV's top electrode. The magnetic field pulses (pump) were synchronized to the light pulses by means of a variable electronic delay  $t$ , yielding a stroboscopic picture of the magnetization pattern [6].

In the ground state the exchange bias forces the microscopic SV elements into an almost uniform magnetization state resulting in a weak contrast in Fig. 1 at  $t = 0$  ps). Only close to the edges the soft layer magnetization turns parallel to the boundaries, thus comprising a positive (negative) value of  $M_x(t)$  and reducing stray field energy. The magnetic field pulse rotates the magnetization  $\vec{M}(\vec{r}, t)$  into the direction of the external field  $\vec{H}_p(t)$  (bright contrast at  $t = 600$  ps). After the pulse has passed,  $\vec{M}(\vec{r}, t)$  rotates through the equilibrium position into the opposite direction (dark contrast at  $t = 600$  ps) and finally back to its initial direction. In order to test the homogeneity of this precessional motion across the structure, we analyzed line profiles (not shown) taken along the diagonal of the structures (marked by the white lines in Fig. 1). These profiles revealed that  $\vec{M}(\vec{r}, t)$  is *not*

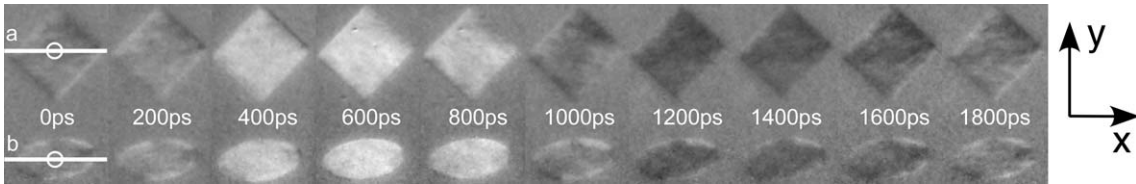


FIG. 1: Sequence of selected domain image snapshots of a quadratic ( $5 \times 5 \mu\text{m}^2$ ) and elliptical ( $6 \times 3 \mu\text{m}^2$ ) SV element acquired at the indicated time delay after the field pulse. The external field (peak value  $\mu_0 H = 1 \text{ mT}$ ; time dependence see Fig. 2(a)) acts along the  $x$  axis, the magnetic easy axis points along  $y$ . The gray level encodes the  $M_x(t)$  magnetization component.

phase-coherent in the case of the square, but rather develops a mode structure as a function of time. In contrast, similar profiles taken across the the ellipse indicated an almost coherent rotation of  $\vec{M}(\vec{r}, t)$  consistent with a macrospin picture. In order to analyze the deviations from the macrospin picture in more detail we compare in Fig. 2(b) the time dependence of  $M_x^m(t)$  averaged over the total field of view with the local value  $M_x^e(t)$  ( $M_x^s(t)$ ) measured in the central circular area of the square (ellipse) (indicated in Fig. 1). At first glance the time dependences  $M_x^i(t)$  are close to each other and resemble that of a critically damped oscillation.

The local variations of  $M_x(t)$  are emphasized in the difference image shown as an inset in Fig. 2(b) and by the differences  $\Delta M_x(t) = M_x^i(t) - M_x^m(t)$  revealing the true discrepancies between averaged and local magnetization dynamics [Fig. 2(c)]. Residual small edge domains that do not participate in the magnetization rotation cause the positive (negative) constant offset of  $\Delta M_x^i(t)$  for the ellipse (square). For the ellipse  $\Delta M_x^e(t)$  reveals a broad maximum coinciding with the strong counter-clockwise rotation of  $\vec{M}(\vec{r}, t)$ . This behavior indicates a slower rebound of  $\Delta M_x^e(t)$  that can be explained by the attenuation of the bias field by the in-plane demagnetization field of the ellipse, which reveals a hard axis parallel to the bias field. Contrarily,  $\Delta M_x^s(t)$  shows an oscillation with a frequency of 1.7 GHz. The difference image shown in the inset of Fig. 2(b) relates this frequency to a spin wave mode identified by the two circularly shaped black areas. The wavelength of this mode along the diagonal amounts to  $3.5 \mu\text{m}$ , i.e. half the value of the diagonal.

The fundamental eigenmode frequency of the square estimated from a similar measurement using smaller and shorter field pulses takes a value of  $f = 0.8 \text{ GHz}$  in the field-free time range. Neglecting lateral demagnetizing fields and assuming a macrospin model the ferromagnetic resonance frequency for exchange biased films is given by  $2\pi f = \gamma \sqrt{M_s H_A}$  with  $H_A = H_{\text{bias}} + H_s$  including the exchange bias field  $H_{\text{bias}}$  and an induced in-plane uniaxial anisotropy  $H_s$ . Under these conditions, the observed eigenmode frequency corresponds to  $H_A = 0.6 \text{ mT}$ , in agreement with the quasistatic value of  $H_{\text{bias}}$  derived from the easy axis magnetization curve.

This example clearly shows the limitations of the macrospin picture in magnetically complex layered systems. For a better understanding of the magnetodynamic behavior and its shape dependence more

detailed micromagnetic descriptions are needed.

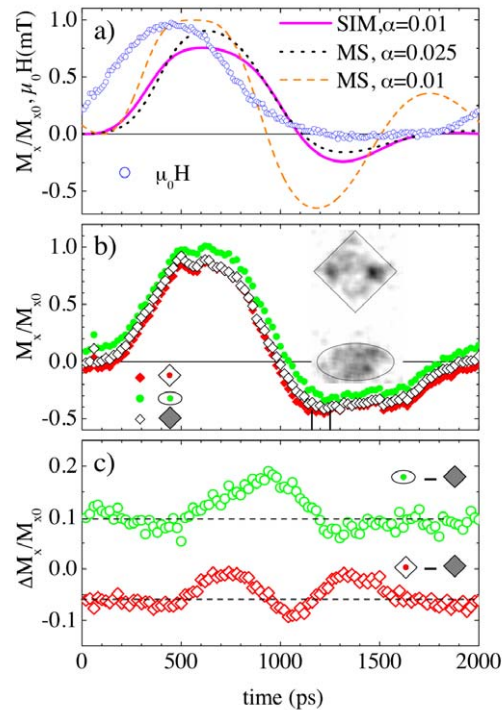


FIG. 2: (a) Experimentally determined field pulse  $H_x(t)$  [o]. Magnetization component  $M_x(t)$  predicted by the macrospin (MS) model at low (dashed line) and high (dotted line) damping coefficients.  $M_x(t)$  calculated by a micromagnetic simulation (SIM) for the square pattern is shown by the full line. (b)  $M_x(t)$  averaged over the entire field of view [ $M_x^m(t)$ ,  $\diamond$ ] and in the central area of the square platelet [ $M_x^s(t)$ ,  $\blacklozenge$ ] and the elliptical particle [ $M_x^e(t)$ ,  $\bullet$ ]. Inset: difference between images acquired at  $t = 1160 \text{ ps}$  and  $1260 \text{ ps}$ . (c) Magnetization variation  $\Delta M_x = M_x^i - M_x^m$  for the central areas of the square [ $\diamond$ ] and ellipse [o].

- [1] P. Grünberg *et al.*, Phys. Rev. Lett. **57**, 2442 (1986).
- [2] S. O. Demokritov *et al.*, Phys. Rep. **348**, 441 (2001).
- [3] F. Wegelin *et al.*, Phys. Rev. B **76**, 134410 (2007).
- [4] M. N. Baibich *et al.*, Phys. Rev. Lett. **61**, 2472 (1988).
- [5] G. Binasch *et al.*, Phys. Rev. B **39**, 4828 (1989).
- [6] G. Schönhense *et al.*, Adv. Imaging Electr. Phys. **142**, 159 (2006).